Inverse Mode Calculations of the Incompressible Turbulent Boundary Layer on an Ellipsoid

S. F. Radwan* and S. G. Lekoudis†
Georgia Institute of Technology, Atlanta, Georgia

The boundary layer equations for three-dimensional, incompressible turbulent flow have been solved using the inverse formulation. In this formulation the displacement thicknesses are prescribed and the pressure distribution results from the calculation. The geometry examined is the ellipsoid of revolution, and the turbulence model used is the anisotropic eddy viscosity. A finite-difference procedure has been used to compute the flow. For the case of the ellipsoid, it was found that the inverse formulation is capable of allowing marching into regions that are inaccessible to calculations that use prescribed pressure. Therefore, it seems feasible to use such a formulation for future viscous/inviscid interaction procedures in order to study three-dimensional separation from smooth surfaces. Also, the procedure provides an alternative to windward differencing for flows with small reversed circumferential flow.

I. Introduction

THE computation of three-dimensional viscous flows is of interest in several areas of fluid mechanics. An arbitrary classification of methods for computing three-dimensional viscous flows is as follows. One way of computing them consists of methods that solve the three-dimensional Navier-Stokes equations. In favor of this category is the increasing memory and speed of the available computers and the simplicity of coding. The second category is that of viscous/inviscid interactions, in which different approximations to the Navier-Stokes equations are being solved for different parts of the flowfield. Usually the thin shear layer equations are used close to the surface of solids. However, the thin shear layer equations, being parabolic, do not allow marching into separated flow regions when the pressure distribution is prescribed. In the past, this restricted the applications of viscous/inviscid interactions to attached flows.

Current interest is directed toward the computation of separated flows. By prescribing the displacement thickness distribution instead of the pressure distribution, in solving the thin shear layer equations, viscous/inviscid interactions are capable of computing flows with separation. This method of solving the thin shear layer equations is called computation in the inverse mode. The advantage of viscous/inviscid interactions methods is primarily their ability of providing good resolution of different parts of the flowfield and the short computing times required, as compared to those required by a Navier-Stokes solver. A number of references about solutions of the two-dimensional boundary layer equations in the inverse mode can be found in Ref. 1. It should be noted that solutions of the boundary layer equations in the inverse mode can be useful in design work.[2,3]

The problem becomes more complicated in three dimensions. One of the reasons is that for a boundary layer calculation, the size of the convection terms depends on the direction of marching. This is a well-known fact and it has been used in the past to increase the capability of marching schemes. In these procedures the differentiation is done so that the domain of dependence of the equations is satisfied as much as possible. The resulting differencing is sometimes called windward differencing. In an inverse procedure for two-dimensional flows, the convection terms that propagate information against the direction of marching are either being neglected or used with a sign change. For three-dimensional flows, besides the fact that the size of the convection terms depends on the direction of marching, it is not known a priori if one needs to neglect all of the convection terms that propagate information against the direction of marching.

A related issue is that of the separation singularity. The problem has been studied in the context of integral boundary layer theory for three-dimensional flows in some detail.[4] Numerical solutions obtained by using finite differences indicate that the numerical "breakdown" occurs close to an area where the wall streamlines focus together into an envelope.[5,11,12] Whether this event should be termed separation or not is a subject for discussion.

Several publications have recently appeared that deal with inverse boundary layer solutions for three-dimensional flow.[1-8] In Refs. 6 and 7 interactive calculations are presented for separated flow on a wing. An integral boundary layer procedure has been used. The authors indicate that in the separated flow region convergence problems had to be overcome by appropriately choosing the parameters that have to be specified in the inverse boundary layer calculation. Thus, an interesting question appears. Do inverse procedures break down at the same location as boundary layer calculations that use prescribed pressure? Is it better to use an inverse procedure, or will traditional windward differencing provide a more powerful method for three-dimensional boundary layer flows?

In order to examine the issues discussed, we solved the boundary layer equations for three-dimensional incompressible flow using both the direct and inverse formulations. With separation from smooth surfaces in mind, we examine the flowfield around an ellipsoid of revolution. This flowfield has been examined before numerically by different investigators.[9-16] Thus a good analytical data base exists and comparisons can be made. In what follows we describe the numerical formulation and procedures used and the results we obtained, ending with concluding remarks.

II. The Analytical Formulation

The coordinate system used in this study is shown in Fig. 1. In this coordinate system x has the value of zero at the nose

Presented as Paper 85-1654 at the AIAA 18th Fluid Dynamics, Plasmadynamics and Lasers Conference, Cincinnati, OH, July 14-18, 1985; received Aug. 19, 1985; revision received Feb. 3, 1986.

*Graduate Research Assistant, School of Aerospace Engineering. Student Member AIAA.

†Associate Professor, School of Aerospace Engineering. Member AIAA.

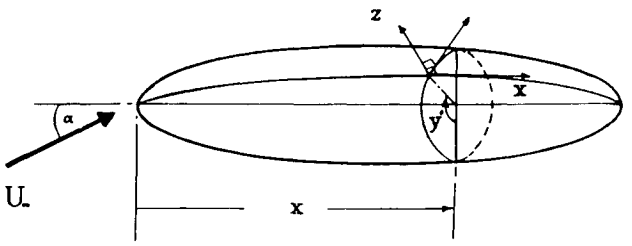

Fig. 1 Surface oriented body coordinate system for the ellipsoid.

of the ellipsoid and two at the end of the ellipsoid, while y has the value of zero at the windward side of the plane of symmetry, and π at the leeward side of the plane of symmetry. In this coordinate system the boundary layer equations for three-dimensional incompressible turbulent flow are as follows:

$$\frac{\partial u}{\partial x} + A_1\frac{\partial v}{\partial y} + A_2\frac{\partial w}{\partial z} + A_3 u + A_4 v = 0 \tag{1a}$$

$$u\frac{\partial u}{\partial x} + B_1 v\frac{\partial u}{\partial y} + B_2 w\frac{\partial u}{\partial z} + B_3 u^2 + B_4 uw + B_5 v^2 = B_6 + B_7\frac{\partial}{\partial z}\left(\frac{\partial u}{\partial z} - \overline{u'w'}\right) \tag{1b}$$

$$u\frac{\partial v}{\partial x} + C_1 v\frac{\partial v}{\partial y} + C_2 w\frac{\partial v}{\partial z} + C_3 u^2 + C_4 uv + C_5 v^2 = C_6 + C_7\frac{\partial}{\partial z}\left(\frac{\partial v}{\partial z} - \overline{v'w'}\right) \tag{1c}$$

Equation (1a) is the continuity equation and Eqs. (1b) and (1c) are the momentum equations in the x and y directions, respectively, and u, v, and w denote the velocity components along the direction of x, y, and z, respectively. The semi-major axis of the ellipsoid a and the freestream velocity u_∞ have been used to nondimensionalize the equations. The z coordinate and the w component of the velocity are scaled by the square root of the reference Reynolds number. The coefficients A_i, B_i, and C_i are known functions of the metric tensor components and their partial derivatives, including the pressure gradient terms, and are listed in Ref. 17.

The boundary conditions for these equations are as follows: At the wall

$$u = v = w = 0 \quad \text{at } z = 0 \tag{2a}$$

At the edge of the boundary layer in the direct mode calculations

$$u = u_e(x, y), \quad v = v_e(x, y) \quad \text{at } z \to \infty \tag{2b}$$

In the calculations done in the inverse mode the following displacement thicknesses were used as input:

$$\delta_x = \frac{u_e}{Q_e}\int_0^\infty \left(1 - \frac{u}{u_e}\right) dz \tag{2c}$$

$$\delta_y = \frac{v_e}{Q_e}\int_0^\infty \left(1 - \frac{v}{v_e}\right) dz \tag{2d}$$

where

$$Q_e^2 = u_e^2 + v_e^2 \tag{2e}$$

In both cases the pressure terms in Eqs. (1) were eliminated by using the Euler equations at the edge of the boundary layer:

$$B_6 = u_e\frac{\partial u_e}{\partial x} + B_1 v_e\frac{\partial u_e}{\partial y} + B_3 u_e^2 + B_4 u_e v_e + B_5 v_e^2 \tag{2f}$$

$$C_6 = u_e\frac{\partial v_e}{\partial x} + C_1 v_e\frac{\partial v_e}{\partial y} + C_3 u_e^2 + C_4 u_e v_e + C_5 v_e^2 \tag{2g}$$

In order to start the calculations, the equations for the three-dimensional stagnation flow were solved. Detailed information about them can be found in Ref. 17. At the plane of symmetry the conditions

$$v = 0, \quad \frac{\partial u}{\partial y} = 0 \tag{3a}$$

apply, and the equations for the plane of symmetry are used:

$$\frac{\partial u}{\partial x} + A_1 g + A_2 w + A_3 u = 0 \tag{3b}$$

$$u\frac{\partial u}{\partial x} + B_2 w\frac{\partial u}{\partial z} + B_3 u^2 = B_6 + B_7\frac{\partial}{\partial z}\left(\frac{\partial u}{\partial z} - \overline{u'w'}\right) \tag{3c}$$

$$u\frac{\partial g}{\partial x} + C_1 g^2 + C_2 w\frac{\partial g}{\partial z} + \bar{C}_3 u^2 + C_4 ug = \bar{C}_6 + C_7\frac{\partial}{\partial z}\left(\frac{\partial u}{\partial z} - \overline{g'w'}\right) \tag{3d}$$

where

$$g = \frac{\partial v}{\partial y} \tag{3e}$$

$$\bar{C}_3 = \frac{\partial C_3}{\partial y} \tag{3f}$$

$$\bar{C}_6 = \frac{\partial C_6}{\partial y} \tag{3g}$$

Equation (3d) is obtained by differentiating Eq. (1c) with respect to y and using the symmetry conditions. The boundary conditions for these equations are

$$u = g = w = 0 \quad \text{at } z = 0 \tag{3h}$$

$$u = u_e, \quad g = g_e \quad \text{at } z \to \infty \tag{3i}$$

Rotta's anisotropic eddy-viscosity model is used for turbulence as follows:

$$\begin{bmatrix} -\overline{u'w'} \\ -\overline{v'w'} \end{bmatrix} = \begin{bmatrix} b_{11} & b_{12} \\ b_{21} & b_{22} \end{bmatrix} \begin{bmatrix} \frac{\partial u}{\partial z} \\ \frac{\partial v}{\partial z} \end{bmatrix} \tag{4a}$$

where

$$b_{11} = \epsilon(u^2 + Tv^2)/Q^2 \tag{4b}$$

$$b_{12} = b_{21} = \epsilon(1 - T)uw \tag{4c}$$

$$b_{22} = \epsilon(v^2 + Tu^2)/Q^2 \tag{4d}$$

$$Q^2 = u^2 + v^2 \tag{4e}$$

ϵ is a scalar eddy viscosity, nondimensionalized with the molecular kinematic viscosity. It is defined in the inner region

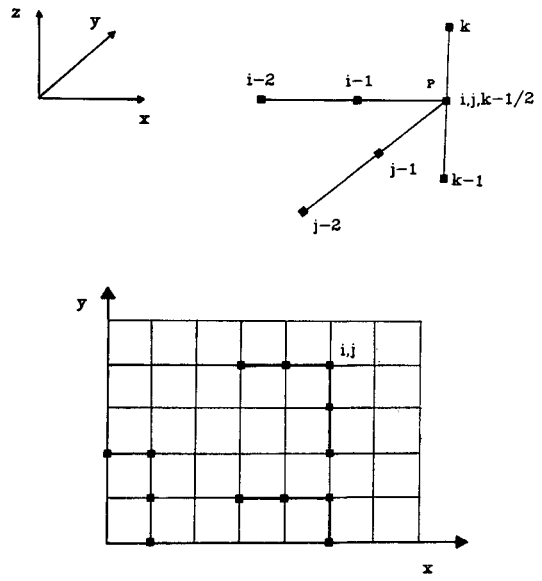

Fig. 2 The computational molecule.

as

$$\epsilon = \sqrt{R_e}\, L^2 \tau \tag{4f}$$

$$L = 0.4z[1 - \exp(-z/A)] \tag{4g}$$

$$\tau^2 = \left(\frac{\partial u}{\partial z}\right)^2 + \left(\frac{\partial v}{\partial z}\right)^2 + (T-1)\left(v\frac{\partial u}{\partial z} - u\frac{\partial v}{\partial z}\right)^2 \Big/ Q^2 \tag{4h}$$

$$A = 26/(1 - 11.8p^+)\, R_e \tau_w^{\frac{1}{2}} \tag{4i}$$

$$\tau^2 = \left(\frac{\partial u}{\partial z}\right)^2 + \left(\frac{\partial v}{\partial z}\right)^2 \quad \text{at } z = 0 \tag{4j}$$

$$p^+ = \left(u_e \frac{\partial Q_e}{\partial x} + V_e \frac{\partial Q_e}{\partial y}\right) \Big/ R_e^{1/4} \tau_w^{3/2} \tag{4k}$$

It is defined in the outer region as

$$\epsilon = 0.0168 R_e \left| \int^{\infty} (Q_e - Q)\, \mathrm{d}z \right| \tag{4l}$$

In the above equation T is the measure of the anisotropy of the model and takes values between zero and one with the isotropic eddy-viscosity result if T is equal to one. For the

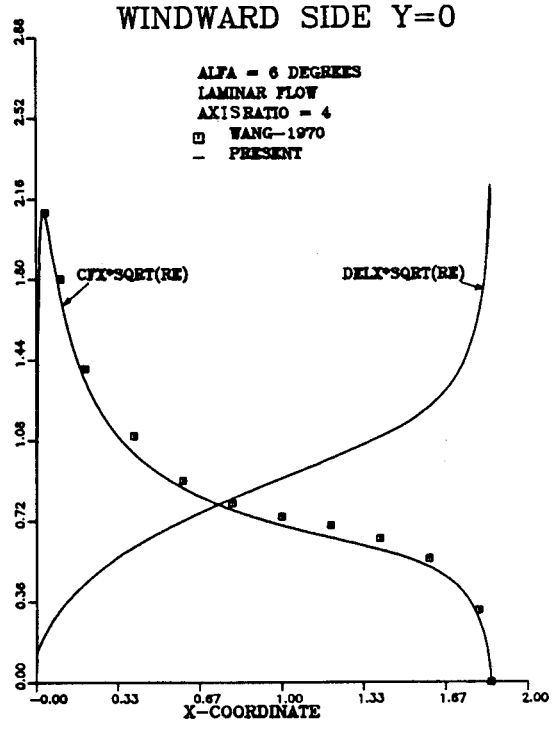

Fig. 3 Windward side solution for laminar flow over a prolate spheroid at 6 deg incidence.

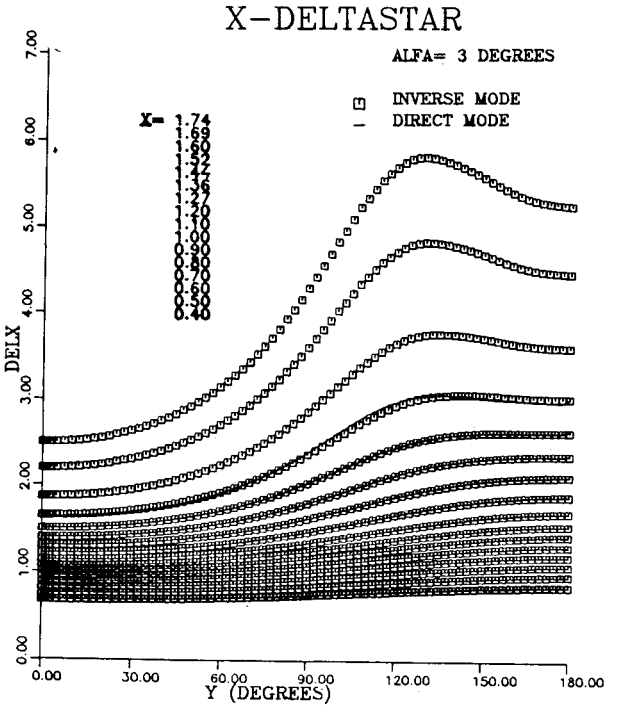

Fig. 5 The extrapolated displacement thickness distribution in the axial direction for laminar flow.

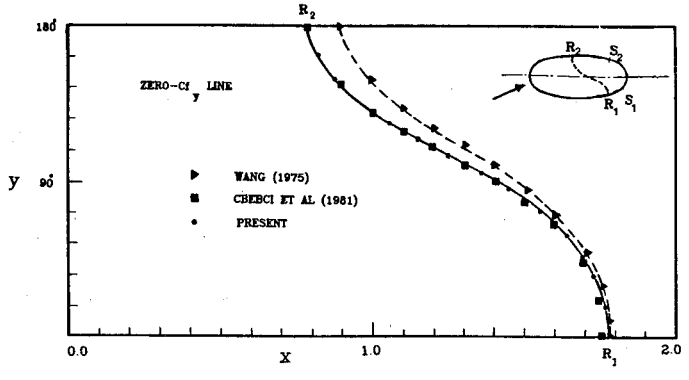

Fig. 4 Direct mode calculations for laminar flow over a prolate spheroid at 6 deg incidence.

case of the plane of symmetry, the model takes the form

$$\begin{bmatrix} -\overline{u'w'} \\ -\overline{g'w'} \end{bmatrix} = \begin{bmatrix} 1 & 0 \\ (1-T)\dfrac{v}{u} & T \end{bmatrix} \begin{bmatrix} \dfrac{\partial u}{\partial z} \\ \dfrac{\partial g}{\partial z} \end{bmatrix} \tag{4m}$$

III. The Numerical Procedure

The procedure used is formerly second-order accurate in the direction normal to the wall, and the accuracy in the x and y directions can be controlled from the input. The differencing of the convection terms is done as follows: for a quantity f

$$\left.\frac{\partial f}{\partial x}\right|_{i,j}^{k-\frac{1}{2}} = a_1 f_i^{k-\frac{1}{2}} + a_2 f_{i-1}^{k-\frac{1}{2}} + a_3 f_{i-2}^{k-\frac{1}{2}} \tag{5a}$$

$$\left.\frac{\partial f}{\partial y}\right|_{i,j}^{k-\frac{1}{2}} = b_1 f_j^{k-\frac{1}{2}} + b_2 f_{j-1}^{k-\frac{1}{2}} + b_3 f_{j-2}^{k-\frac{1}{2}} \tag{5b}$$

$$\left.\frac{\partial f}{\partial z}\right|_{ij}^{k-\frac{1}{2}} = \frac{1}{\Delta z_k}\left(f^k - f^{k-1}\right) \tag{5c}$$

$$f^{k-\frac{1}{2}} = \tfrac{1}{2}\left(f^k + f^{k-1}\right) \tag{5d}$$

$$a_1 = \frac{1-r}{\Delta x_i} + r\frac{2\Delta x_i + \Delta x_{i-1}}{\Delta x_i(\Delta x_i + \Delta x_{i-1})} \tag{5e}$$

$$a_2 = \frac{1-r}{\Delta x_i} - r\frac{(\Delta x_i + \Delta x_{i-1})}{\Delta x_i \Delta x_{i-1}} \tag{5f}$$

$$a_3 = r\frac{\Delta x_i}{\Delta x_{i-1}(\Delta x_i + \Delta x_{i-1})} \tag{5g}$$

The value of the upwinding parameter r, between zero and one, is controlled from input. The coefficients b_i are the same as the a_i with Δy replacing Δx. Also

$$\Delta x_i = x_i - x_{i-1} \tag{5h}$$

$$\Delta y_j = y_j - y_{j-1} \tag{5i}$$

$$\Delta z_k = z_k - z_{k-1} \tag{5j}$$

The governing differential equations have been discretized at the location $i, j, k^{-\frac{1}{2}}$ (see Fig. 2). Different windward differencing schemes have been applied in the direct mode calculations and details can be found in Ref. 17. We only describe a scheme based on the method of characteristics[17] that has been used to generate the direct mode results presented here. Because the solution proceeds from the windward line of symmetry, whenever v is negative, the inertia terms in the momentum equations are written in the local streamline coordinate system. The inertia terms in Eqs. (1b) and (1c) become

$$u\frac{\partial u}{\partial x} + B_1 v\frac{\partial u}{\partial y} = \Lambda\frac{\partial u}{\partial s} \tag{6a}$$

$$u\frac{\partial v}{\partial x} + C_1 v\frac{\partial v}{\partial y} = \Lambda\frac{\partial v}{\partial s} \tag{6b}$$

where

$$\Lambda^2 = u^2 + \left(vh_x/h_y\right)^2 \tag{6c}$$

The derivatives along the streamline direction s are then evaluated using the procedure described by Eqs. (5). The values of u and v at point w off the grid points are obtained by quadratic interpolation.

The system of Eqs. (1) is transformed into a set of first-order equations by using the components F_1 and F_2 of the scaled vector potential

$$u = U_1 = \frac{\partial F_1}{\partial z} \qquad v = U_2 = \frac{\partial F_2}{\partial z} \tag{7a}$$

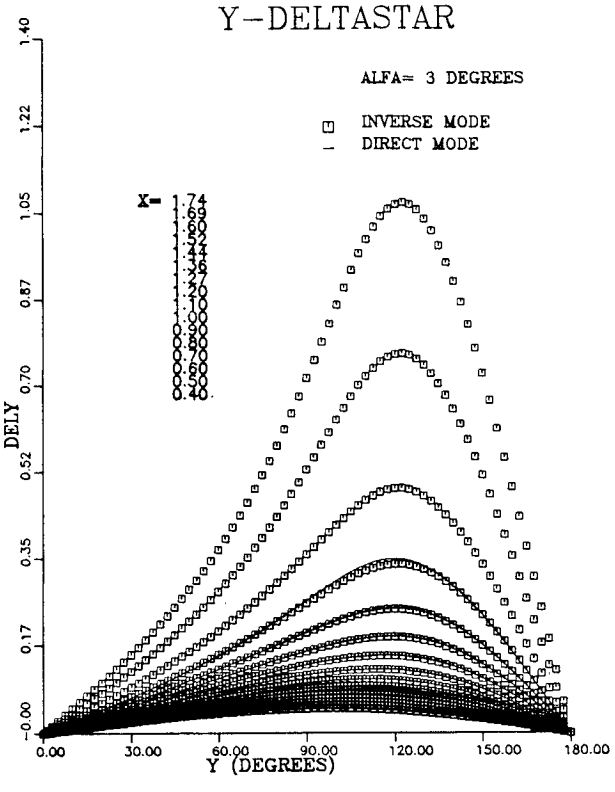

Fig. 6 The extrapolated displacement thickness distribution in the circumferential direction for laminar flow.

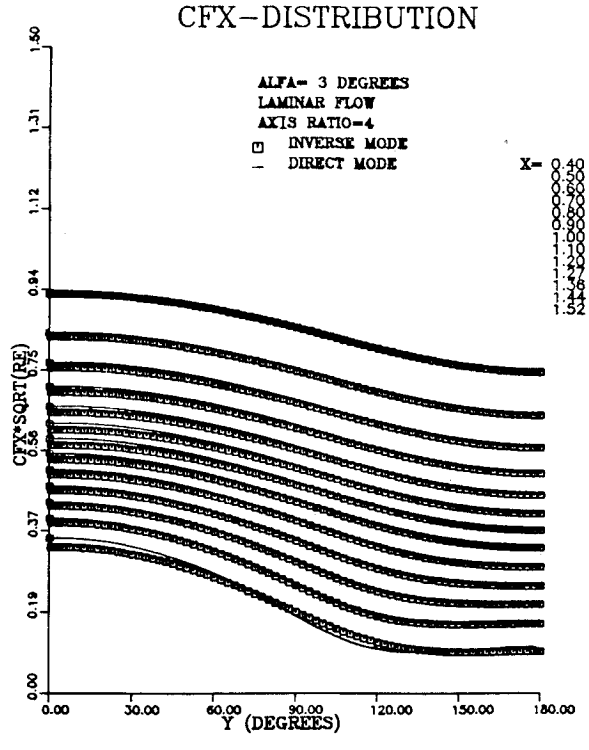

Fig. 7 Comparison between inverse mode and direct mode laminar calculations for the skin friction coefficient component c_{fx}.

$$\frac{\partial u}{\partial z} = V_1 \qquad \frac{\partial v}{\partial z} = V_2 \tag{7b}$$

$$u_e = W_1 \qquad v_e = W_2 \tag{7c}$$

Then, using the closure model for turbulence described in the last section, the governing equations can be written as a system of first-order-coupled partial-differential equations and they are listed in the Appendix. The boundary conditions for these equations are as follows: At the wall

$$F_1 = F_2 = U_1 = U_2 = W = 0 \quad \text{at } z = 0 \tag{8a}$$

At the edge of the boundary layer

$$W_1 = U_1, \quad W_2 = U_2 \quad \text{at } z = z_e \tag{8b}$$

Moreover, if the calculations are done in the direct mode, then the values for the edge velocities U_e and V_e are known and prescribed. In the inverse mode the following boundary conditions are used

$$F_1 - \gamma_1 W_1 = 0 \quad \text{at } z = z_e \tag{8c}$$

$$F_2 - \gamma_2 W_2 = 0 \quad \text{at } z = z_e \tag{8d}$$

where

$$\gamma_1 = z_e - (Q_e \delta_x / W_1) \tag{8e}$$

$$\gamma_2 = z_e - (Q_e \delta_y / W_2) \tag{8f}$$

where the δ_x and δ_y are defined in Eqs. (2c) and (2d).

The systems of equations in the Appendix are discretized using Eq. (5). The resulting difference equations are coupled and nonlinear and they are solved using the (4×4) block elimination method of Cebeci and Keller.[11] Then each transformed momentum equation was solved separate from the other using the block elimination method. The continuity equation (7d) is used to obtain w and iterations are carried out because of the nonlinearity. Different convergence tests were used and a good one is the convergence of the wall slope of the velocity profile. The slope at the edge of the boundary layer was checked and, if larger than a prescribed value, more points were added to the grid.

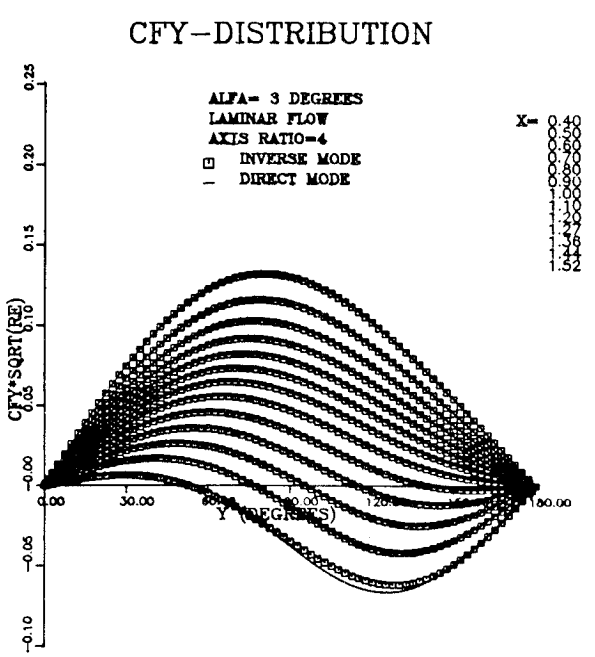

Fig. 8 Comparison between inverse mode and direct mode laminar calculations for the skin friction coefficient component c_{fy}.

IV. Results and Discussion

Before any discussion of the calculations in the inverse mode is made, it is proper to examine if the boundary layer code reproduces existing results for the flow around the ellipsoid. Different investigators developed different methods for computing in the nose region, and the most sophisticated one is described in Ref. 5. In the present work the computations in the nose region are as follows. The stagnation location is found, for a given angle of attack, from the closed form solution of the potential flow around the ellipsoid.[18] The equation for three-dimensional stagnation flow is then solved,[17] using the same algorithm that is described in Sect. III of this paper. Then, at the x location of the stagnation point, and at all y locations, the velocity profiles of the stagnation flow are used, after they have been scaled, so that the local freestream velocity vector is that obtained from the potential flow solution. This treatment of the nose region limits the accuracy of the calculations in the nose region. However, for the case of turbulent flow, it should not significantly affect the solution downstream.

We compared laminar flow results with results obtained by other investigators. Figure 3 shows the derivative of the velocity profile at the wall, along the windward line of symmetry. Figure 4 shows the location of the reversal of the wall shear

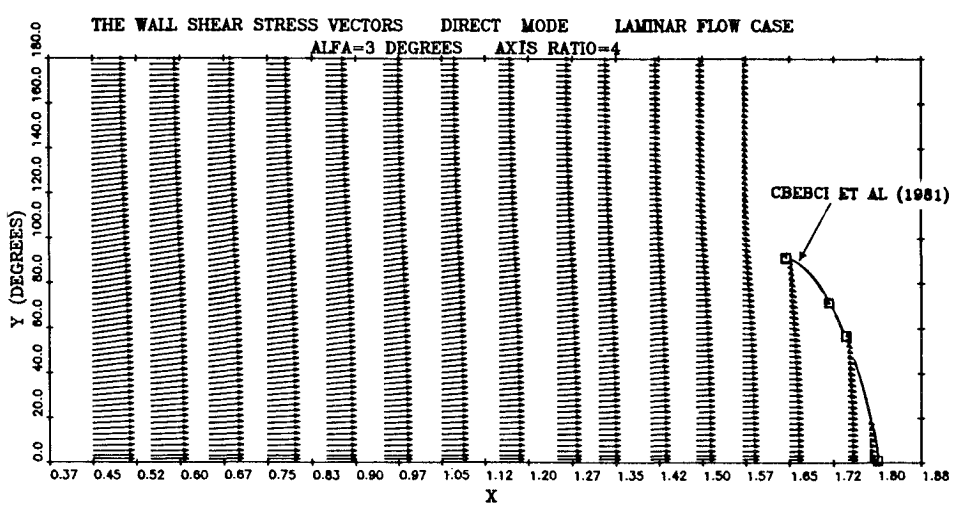

Fig. 9 The computed wall shear stress vectors in the direct mode for laminar flow.

component along the y direction. These results are for an ellipsoid with ratio of axes four, and at six degrees angle of attack. The angle of attack is defined as the angle between the freestream and the axis of symmetry of the ellipsoid. It is evident from these figures that the present formulation in the direct mode of calculation reproduces accurately previous results.

The main objective of this work is to perform calculations in the inverse mode. In order to do it, the problem has been solved backwards. The displacement thicknesses obtained from direct mode calculations were used, as input for the inverse mode calculations. These displacement thicknesses are shown in Figs. 5 and 6. The calculations are for the ellipsoid discussed before, at three degrees angle of attack. Figures 5 and 6 indicate that there is a region at the back end of the ellipsoid, that is inaccessible to direct mode calculations. This agrees with previous calculations.[11,12] Notice that no effort was made to reduce that region by marching from the leeward plane of symmetry. All calculations presented in this paper are done by marching from the windward plane of symmetry.

In order to complete the calculation, displacement thicknesses inside the inaccessible region were constructed by extrapolating the results from the accessible region. The values used are shown in Figs. 5 and 6. Figures 7 and 8 show the computed components of the skin friction vector using both the direct and inverse formulations. In the inverse formulation the convection terms in the circumferential and in the axial direction that propagate information against the marching direction were neglected. The skin friction vectors are plotted in Figs. 9 and 10. These results show that the two formulations produce identical results. Moreover, the inverse formulation is capable of producing results in the region of the ellipsoid that is not accessible to the direct mode procedure. Figures 11 and 12 show some velocity profiles for different y

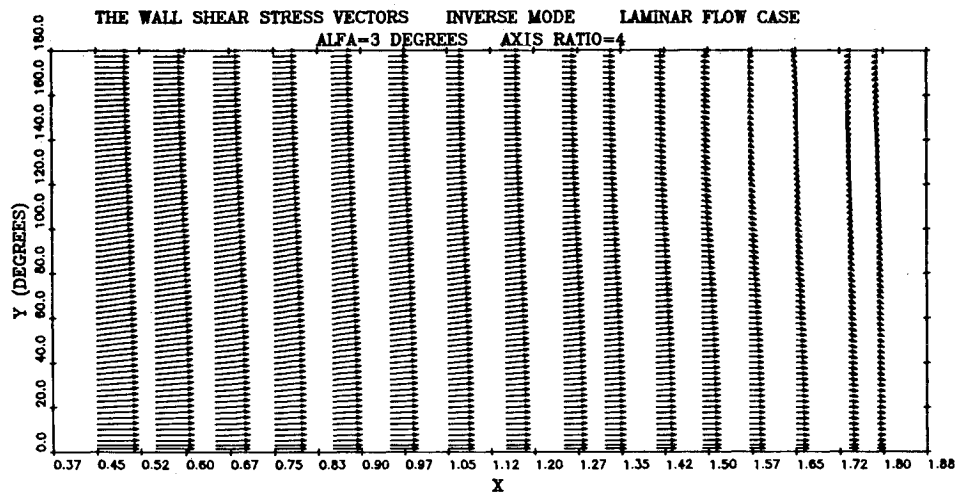

Fig. 10 The computed wall shear stress vectors in the inverse mode for laminar flow.

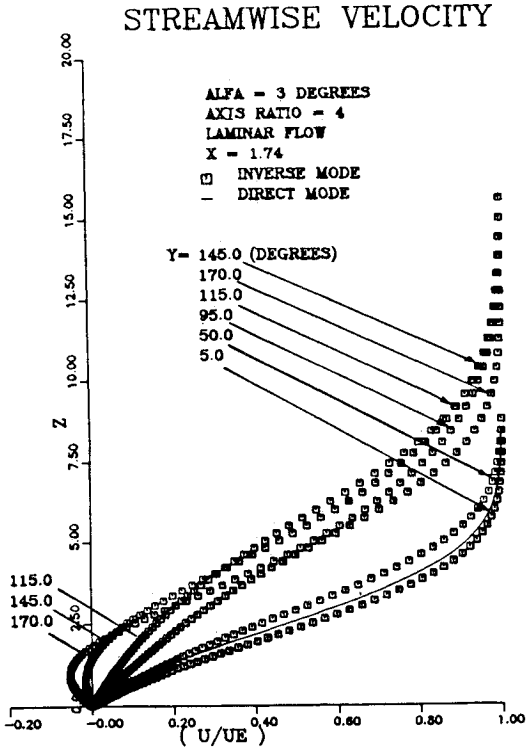

Fig. 11 Inverse mode calculations for the axial velocity profiles inside the regions inaccessible to direct mode calculations.

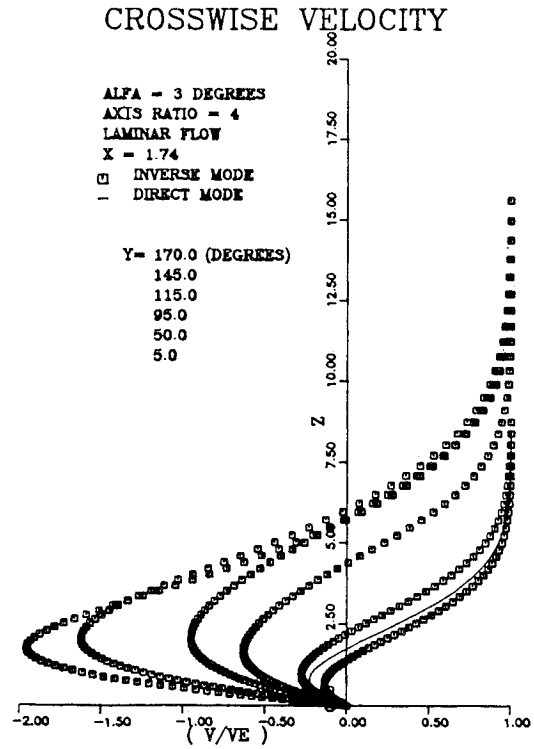

Fig. 12 Inverse mode calculations for the circumferential velocity profiles inside the regions inaccessible to direct mode calculations.

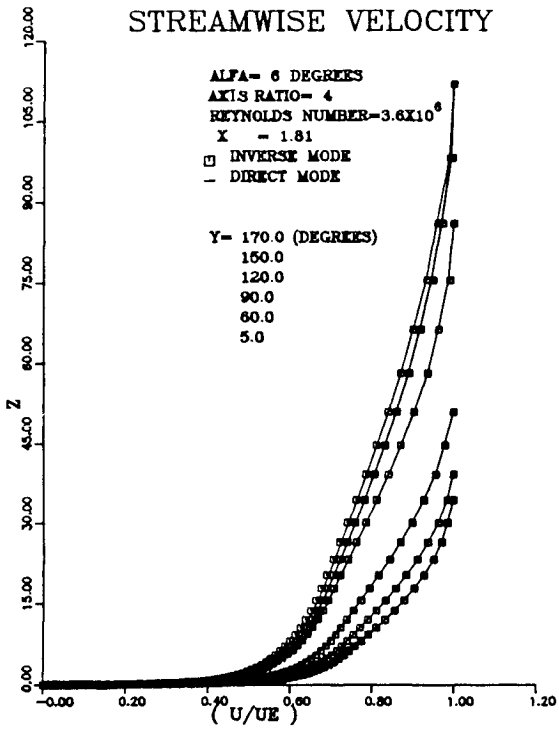

Fig. 13 Comparison between inverse mode and direct mode turbulent calculations.

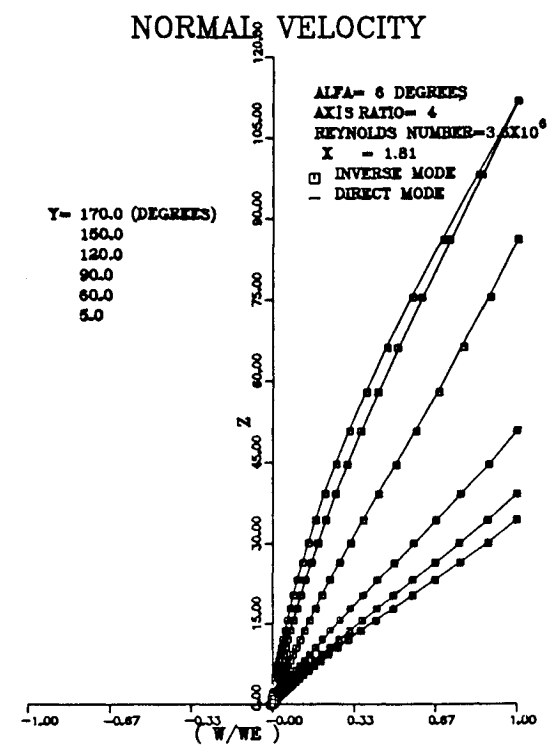

Fig. 15 Comparison between inverse mode and direct mode turbulent calculations.

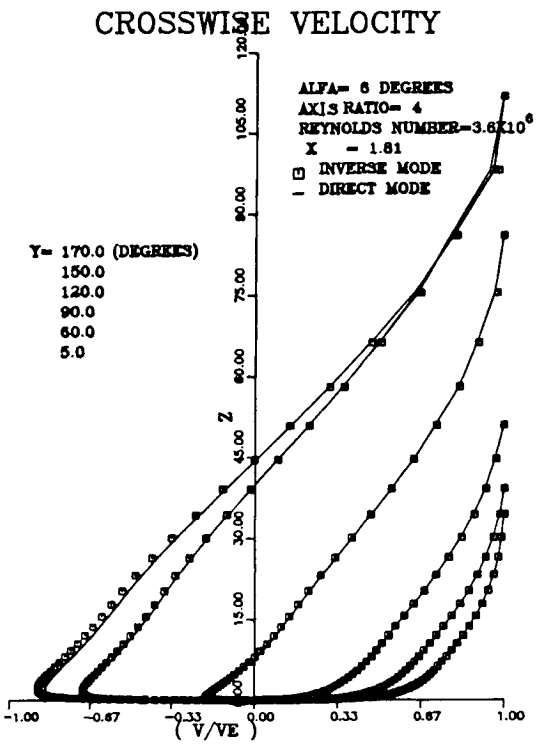

Fig. 14 Comparison between inverse mode and direct mode turbulent calculations.

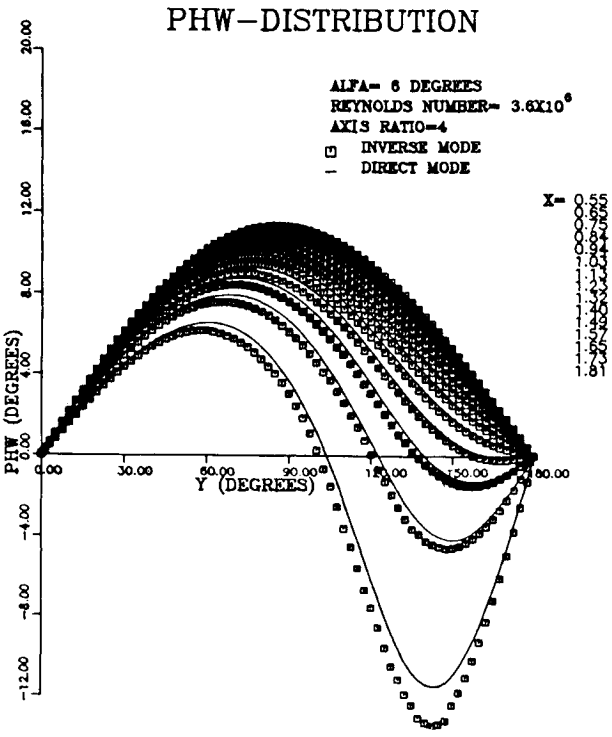

Fig. 16 Comparison between inverse mode and direct mode turbulent calculations for the flow angle at the wall.

locations and for an x location close to the trailing edge. Notice that both components of the velocity indicate flow reversal. The reader should be reminded that windward differencing has been used in all of the calculations that use the direct mode. Unless this is done, the area that is accessible to the direct mode results is reduced.

Finally, calculations for turbulent flow are shown in Figs. 13-16. Again, the agreement between direct and inverse mode results is excellent; many more can be found in Ref. 17.

A comment about the behavior of the code is appropriate. It was found that the calculations are sensitive to the smoothness of the input displacement thicknesses. The experience of the authors suggest that this is a manifestation of the way the edge boundary condition is applied and it has nothing to do with the inverse formulation. If the resulting edge velocity is approached by using repeated "inner loop" iterations in the direct mode,[2,3] the code is more robust. It should be mentioned that the best results, in the region of the negative

circumferential flow, were obtained when the marching scheme is close to first-order accurate in the marching direction.

V. Conclusions

Inverse mode calculations for the three-dimensional boundary on an ellipsoid of revolution at incidence, for incompressible laminar and turbulent flow, indicate the following:

1) The scheme produces the same results as do windward marching schemes for the case of reversed circumferential flow.

2) These calculations, for the case examined, extend the regions of accessibility for marching schemes that use the boundary layer equations. Therefore, they could be used in future three-dimensional viscous/inviscid interaction procedures.

Appendix

$$\frac{\partial U_1}{\partial x} + A_1\frac{\partial U_2}{\partial y} + A_2\frac{\partial W}{\partial z} + A_3U_1 + A_4U_2 = 0 \quad \text{(A1)}$$

$$\frac{\partial F_1}{\partial z} = U_1 \quad \text{(A2)}$$

$$\frac{\partial U_1}{\partial z} = V_1 \quad \text{(A3)}$$

$$B_7\frac{\partial}{\partial z}(\bar{b}_{11}V_1) + B_7\frac{\partial}{\partial z}(\bar{b}_{12}V_2) - B_2WV_1 - U_1\frac{\partial U_1}{\partial x} - B_1U_2\frac{\partial U_1}{\partial y} - B_3U_1^2 - B_4U_1U_2 - B_5U_2^2 - W_1\frac{\partial W_1}{\partial x} - B_1W_2\frac{\partial W_2}{\partial y} - B_3W_1^2 - B_4W_1W_2 - B_5W_2^2 = 0 \quad \text{(A4)}$$

$$\frac{\partial W_1}{\partial z} = 0 \quad \text{(A5)}$$

$$\frac{\partial F_2}{\partial z} = U_2 \quad \text{(A6)}$$

$$\frac{\partial U_2}{\partial z} = V_2 \quad \text{(A7)}$$

$$C_7\frac{\partial}{\partial z}(\bar{b}_{22}V_2) + C_7\frac{\partial}{\partial z}(\bar{b}_{21}V_1) - C_2WV_2 - U_1\frac{\partial U_2}{\partial x} - C_1U_1\frac{\partial U_2}{\partial y} - C_3U_1^2 - C_4U_1U_2 - C_5U_2^2 - W_1\frac{\partial W_2}{\partial x} - C_1W_1\frac{\partial W_2}{\partial y} - C_3W_1^2 - C_4W_1W_2 - C_5W_2^2 = 0 \quad \text{(A8)}$$

$$\frac{\partial W_2}{\partial z} = 0 \quad \text{(A9)}$$

where

$$\bar{b}_{11} = 1 + \epsilon\left(U_1^2 + TU_2^2\right)/Q^2 \quad \text{(A10)}$$

$$\bar{b}_{12} = \bar{b}_{21} = \epsilon(1-T)U_1U_2/Q^2 \quad \text{(A11)}$$

$$\bar{b}_{22} = 1 + \epsilon\left(U_2^2 + U_1^2\right)/Q^2 \quad \text{(A12)}$$

Acknowledgment

This work was supported by the Advanced Research Organization of the Lockheed-Georgia Company.

References

[1] Radwan, S.F. and Lekoudis, S.G., "Boundary Layer Calculations in the Inverse Mode for Incompressible Flows Over Infinite Swept Wings," *AIAA Journal*, Vol. 22, June 1984, pp. 737-743.

[2] Lekoudis, S.G., Sankar, L.N., and Radwan, S.F., "A Method for Designing Three-Dimensional Configurations with Prescribed Skin Friction," *Journal of Aircraft*, Vol. 21, Nov. 1984, pp. 924-926.

[3] Lekoudis, S.G., Sankar, N.L., and Malone, J.B., "The Application of Inverse Boundary Layer Methods to the Three-Dimensional Viscous Design Problem," *Communications in Applied Numerical Methods*, Vol. 2, pp. 57-61, 1986.

[4] Cousteix, J. and Houderville, R., "Singularities in Three-Dimensional Turbulent Boundary-Layer Calculation and Separation Phenomena," *AIAA Journal*, Vol. 19, Aug. 1981, pp. 976-985.

[5] Delery, J.M. and Formery, M.J., "A Finite Difference Method for Inverse Solutions of 3-D Turbulent Boundary Layer Flow," AIAA Paper 83-0301, Jan. 1983.

[6] Wington, L.B. and Yoshihara, H., "Viscous-Inviscid Interactions with a Three-Dimensional Inverse Boundary Layer Code," *Proceedings of the Second Symposium on Numerical and Physical Aspects of Aerodynamic Flows*, California State University, Long Beach, Jan. 1983.

[7] Yoshihara, H. and Wai, J., "Transonic Turbulent Separation on Swept Wings—A Return to the Direct Formulation," AIAA Paper 84-0265, Jan. 1984.

[8] Piquet, J. and Visoneau, M., "Inverse Mode Solution of the Three-Dimensional Boundary Layer Equations About a Shiplike Hull," *Proceedings of the Third Symposium on Numerical and Physical Aspects of Aerodynamic Flows*, California State University, Long Beach, Jan. 1985.

[9] Ragab, S.A., "A Method for Calculation of Three-Dimensional Boundary Layers with Circumferential Reversed Flow on Bodies," AIAA Paper 82-1023, June, 1982.

[10] Ragab, S.A., "Euler/Boundary Layer Solutions for Vortex Separation from Smooth Surfaces," AIAA Paper 85-0016, Jan. 1985.

[11] Cebeci, T., Khattab, A.K., and Stewartson, K., "Three-Dimensional Laminar Boundary Layers and the OK of Accessibility," *Journal of Fluid Mechanics*, Vol. 107, 1981, pp. 57-87.

[12] Wang, K.C., "Boundary Layer Over a Blunt Body at Low Incidence with Circumferential Reversed Flow," *Journal of Fluid Mechanics*, Vol. 72, Part 1, 1975, pp. 49-65.

[13] Petel, V.C. and Baek, J.H., "Calculation of Boundary Layers and Separation on a Spheroid at Incidence," *Proceedings of the Second Symposium on Numerical and Physical Aspects of Aerodynamic Flows*, California State University, Jan. 1983.

[14] Meier, H.V. and Cebeci, T., "Flow Characteristics of a Body of Revolution at Incidence," *Proceedings of the Third Symposium on Numerical and Physical Aspects of Aerodynamic Flows*, California State University, Jan. 1985.

[15] Blottner, F.G. and Ellis, M.A., "Finite-Difference Solution of the Incompressible Three-Dimensional Boundary Layer Equations for a Blunt Body," *Computers and Fluids*, Vol. 1, 1973, pp. 133-158.

[16] Geissler, W., "Three-Dimensional Laminar Boundary Layer Over a Body of Revolution at Incidence and with Separation," *AIAA Journal*, Vol. 12, Dec. 1974, pp. 1743-1745.

[17] Radwan, S.F., "Numerical Solution of the Three-Dimensional Boundary Layer Equations in the Inverse Mode Using Finite-Differences," Ph.D. Dissertation, School of Aerospace Engineering, Georgia Institute of Technology, 1985.

[18] Lamb, M.A., *Hydrodynamics*, Dover Publications, 1932.